



Stability analysis of the underground infrastructure for pumped storage hydropower plants in closed coal mines



Javier Menéndez^{a,*}, Falko Schmidt^b, Heinz Konietzky^c, Jesús M. Fernández-Oro^d, Mónica Galdo^d, Jorge Loredo^e, María B. Díaz-Aguado^e

^a Hunaser Energy, Oviedo 33005, Spain

^b Geotechnical Engineer, Santander 39011, Spain

^c Geotechnical Institute, TU Bergakademie Freiberg, 09599 Freiberg, Germany

^d Energy Department, University of Oviedo, Gijón 33271, Spain

^e Mining Exploitation Department, University of Oviedo, Oviedo 33004, Spain

ARTICLE INFO

Keywords:

Closed coal mine
Energy storage
Hydropower plant
Underground reservoir
Powerhouse cavern
Tunnels network

ABSTRACT

Electricity storage systems are necessary to increase the efficiency of variable renewable energies. Mine water in closed underground coal mines can be used for underground pumped-storage hydropower plants. Subsurface energy storage systems require the excavation of a powerhouse cavern and a network of tunnels as lower water reservoir. To prevent build-up of high air pressures in the network of tunnels during the water filling process it is necessary to excavate ventilation shafts. In this paper, fluid dynamics and geomechanical behavior are combined in the lower reservoir in order to know the feasibility of the underground infrastructure. Depending on the diameter of the ventilation shafts and water flow rate, air pressures up to 420 kPa can be reached. The stability of the powerhouse cavern and the effect of air pressure on the tunnels and shafts during the operation phase of the turbine are analyzed. Coal mines in Northern Spain have been selected as a case study to investigate the behavior of the underground infrastructure of a hydropower plant. Three-dimensional numerical models were developed and analyzed for different rock mass scenarios. The results obtained show that the effect of air pressure on the tunnels and shafts is moderate. The direction of air flow switches during operation time and long-term fatigue damage could be produced to the contour of excavations. The excavation of the powerhouse cavern is technically feasible in case of the application of a proper designed support system.

1. Introduction

Pumped Storage Hydropower (PSH) is the most mature and widely used technology for large-scale energy storage. It accounts for 99% of the current storage capacity. The efficiency of the pumped hydro systems (i.e. energy output to energy absorbed for pumping) is between 70% and 80% (Schoenung et al., 1996; Ibrahim et al., 2008; Yang and Jackson, 2011). PSH plants can start operation and reach full load in few minutes. However, PSH plants can have also negative impacts on landscape, environment and society (Wong, 1996; Kucukali, 2014).

A possible solution to this problem is provided by the idea to install Underground Pumped-Storage Hydropower (UPSH) plants in abandoned mines. The first UPSH scheme was proposed in 1901 (Fessenden, 1907). During 1980's a project to install an UPSH plant was launched in the Netherlands (Braat et al., 1985). A study was carried out to evaluate the potential of ten sites to establish an underground taconite mine in

Minnesota (USA) whose cavities would be used afterwards as lower reservoir for an UPSH plant (Severson, 2011). In Germany, in the Ruhr and Harz regions, UPSH plants have been considered for abandoned coal mines (Luick et al., 2012; Niemann et al., 2015). Although numerous studies of UPSH plants have been carried out, projects of this type have never been put into operation so far.

An UPSH plant consists in two reservoirs: an upper reservoir at the surface and an underground lower reservoir. Although the cheapest alternative would be the usage of abandoned mine workings, due to the current state of the mining drifts, the tunnel network of the lower reservoir should be excavated.

There a number of uncertainties associate with the use of abandoned mines as lower reservoir for UPSH plants that need to be addressed in a feasibility study (Menendez et al., 2019; Winde et al., 2016). Many of those mines are flooded and its use as energy storage plants may be unfeasible. UPSH schemes are suitable in non-flooded

* Corresponding author.

E-mail address: jmenendezr@hunaser-energia.es (J. Menéndez).

mines, where the maintenance costs are lower. In addition, the condition of the mining infrastructure, such as shafts, hoists and ventilation system, should be analyzed. New equipment could be installed but it would imply a significant investment cost. The current vertical shafts would be used in the operation phase. Due to the dimensions and the weight of the equipment of an UPSH plant (Francis pump-turbine and motor-generator), the construction of a new access to transport the equipment from outside to the powerhouse cavern would be necessary.

Tunneling in abandoned coal mines could cause severe geo-environment problems (Tong et al., 2013). The presence of residual voids after cessation of mine activities, which can be filled with water, debris and gas, can have serious consequences on the excavation of tunnels. Due to these problems, areas not affected by abandoned mine workings should be selected to carry out the excavations. The new underground infrastructure has a larger cross section compared with conventional mine workings. Therefore, it is necessary to analyze the technical feasibility of this type of excavations in the rock mass conditions of the Asturian Central Coal Basin (ACCB). In addition to the network of tunnels, the main underground structure of an UPSH plant is the powerhouse cavern, where Francis turbine-pump and motor-generator will be installed.

Although there are already a few studies about UPSH plants, none of them deal with the detailed investigation of the air pressure flow inside the underground reservoir. In this work, the analysis of the air flow inside the reservoir is combined with the effect on the stability of the excavations in the operation phase. In addition, during the operation phase the direction of the air flow switches depending on the operating mode of the hydroelectric power plant: turbine or pumping mode. Due to these changes, the contour of the excavations is subjected to small cyclic tensile loading and long-term fatigue damage could be produced.

This paper analyses the stability of the powerhouse cavern in the rock mass existing of two different underground coal mines in the ACCB. The effect of air pressure on the stability of tunnels and shafts during the operation phase of the turbine, and how it is influenced by diameter and water flow rate, is investigated.

2. Materials and methods

2.1. Study area

The study area is located in the ACCB in NW Spain (Fig. 1). It has an extension of about 1400 km². ACCB is an extensively mined area and its network of tunnels covers more than 30 mines. Two closed underground coal mines (Mine I and Mine II) have been selected as case study to investigate the stability of underground infrastructure of UPSH plants during the construction and operation phases. The typical structure of underground coal mines consists of a main vertical shaft for access and extraction of coal, and networks of horizontal drifts at different levels. There are also auxiliary shafts for the ventilation system and to serve as emergency exits. The depth of the mining operations

reached 600 m below surface. The diameter of the access and ventilation shafts is 6 m. The cross section of the drifts is between 9 and 12 m². The exploitation drifts normally have a support system consisting of steel arches and wire mesh.

2.2. Geology and hydrogeology

The ACCB is characterized by the so-called Sinorogic succession of the Carboniferous, whose age ranges from Tournaisian to Westfalian D. There are shales and sandstones with abundant layers of exploitable coal and some limestones located preferably close to the base. In the middle and upper part some layers of conglomerates up to 60 m thick are interspersed, with clasts exclusively siliceous in the lower horizons, and siliceous and calcareous clasts in the upper horizons.

From the hydrogeological point of view, the ACCB is characterized by low porosity and permeability. Mining activity has induced important changes of the hydrogeological parameters. Porosity, permeability and transmissivity increased significantly: porosity from 1 to more than 10%, permeability from 10⁻¹ to 100 m·day⁻¹, and transmissivity from 10 to 1000 m²·day⁻¹ (Pendas and Loredo, 2006). Underground water has a bicarbonate content between 558 and 725 mg L⁻¹, 160–173 mg L⁻¹ of dissolved sodium and 54–116 mg L⁻¹ of dissolved calcium. Total hardness is between 3 and 5 mg CaCO₃ L⁻¹. The pH value is between 7.2 and 9.4 and the conductivity is 1.2 µS·cm⁻¹ at 20 °C.

2.3. UPSH scheme

The powerhouse caverns are located at a depth of about 450 m. An analysis was made considering the excavation of the powerhouse and the lower reservoir in sandstones and shales rock masses. An UPSH scheme differs from a conventional PSH scheme in the location of the lower reservoir. The scheme of an UPSH plant in a closed underground coal mine is shown in Fig. 2. The upper reservoir is located at the surface and the lower reservoir is excavated in form of a connected tunnel system. To minimize the surface area occupied, the reservoir design has a central tunnel and a number of transversal tunnels on either side which are spaced 20 m apart. The length of these tunnels is about 200 m and the cross section about 30 m² (5 m wide and 6.5 m high). The penstock reaches the powerhouse through the existing vertical shaft. The model also considers the submergence required by the turbine (45 m), through a tunnel with an inclination of 10%. Francis turbine-pump, motor generator and the valve guard are located in the powerhouse. The cross section of power house cavern with semicircular roof and straight wall is 325 m² (50 m long, 12 m wide and 28 m high). The storable amount of energy depends on the net head and the water mass moved. To absorb overpressure during transients in pumping operation, a surge tank of 4 m diameter has been designed. At the end of the lower reservoir, a ventilation shaft evacuates the air during the operation phase.



Fig. 1. Location of Mine I and Mine II in the ACCB, NW Spain.

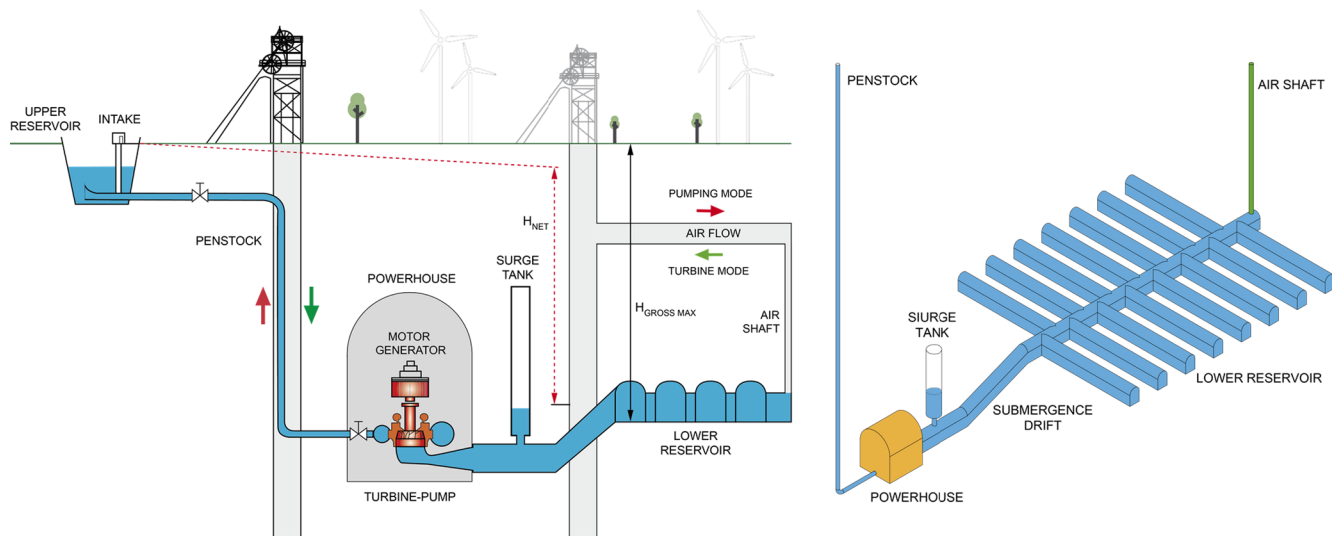


Fig. 2. Scheme of UPSH in a closed underground mine: upper and lower reservoir, penstock, spherical valve, Francis pump-turbine, motor-generator, surge tank and vent shaft (left). 3D detail of the lower reservoir (right).

The air inside the underground reservoir becomes compressed during the filling process. When the air pressure increases, the net head of the UPSH plant decreases, implying a reduction in the production of electrical energy. The air flow passes through the ventilation shaft. The direction of the air flow varies depending on the operation mode of the hydroelectric power plant. The air enters the mine during the pumping mode and leaves the mine during the turbine operation mode. Flow rate and pressure of air depend on the water flow rate of the Francis turbine and the diameter of the ventilation shaft (Menéndez et al., 2019b). These pressure values have been obtained from both analytical and CFD three-dimensional models developed to know the effect of air pressure during the operation of an UPSHP as a function of the number and diameter of ventilation shafts (Menéndez et al., 2019c). The unsteady evolution of the air pressure during the filling and depletion processes was simulated to estimate the peak values, which are used to evaluate the mechanical stability of the infrastructure. The air pressure reaches values up to 420 kPa for a water flow rate of $55 \text{ m}^3 \text{ s}^{-1}$ assuming a diameter of the ventilation shaft of 0.5 m (Menéndez et al., 2019c). The air pressure decreases to 120 kPa for a vent shaft with 1 m diameter. In both operation modes (turbine and pump), the maximum value of the air pressure is reached at the junction of the vent shaft with the tunnel. The value is decreasing when it passes through the shaft to the ground surface. Table 1 shows the parameters selected for the project.

3. Numerical modeling and material properties

FLAC3D software was used to calculate the deformations and the failure states of the powerhouse caverns considering the excavation stages and the rock support (Ray, 2009; Uddin and Asce, 2003). Thus, in the tunnels and ventilation shafts of the lower reservoir the effect of the air pressure due to the operation of the turbine is simulated. To

analyze the stability of the underground infrastructures, two types of 3D models have been developed: one for the excavation of the powerhouse cavern and another which includes a tunnel and a ventilation shaft to study the effect of air pressure.

3.1. Model geometries, meshes and boundary conditions

The powerhouse cavern model is 90 m long, 100 m wide and 100 m high. The number of zones of the model is 63,840. The tunnel and shaft model is 80 m long, 80 m wide and 115 m high. This model has 200,345 zones. In both models roller boundaries are applied at the bottom and along the vertical sides. That means no normal displacements occur at these boundaries. A uniform vertical stress corresponding to the overburden weight is applied at the top. To increase the accuracy of the calculations, the mesh was refined close to the excavations and became gradually coarser outwards. In the powerhouse cavern model, the mesh size (gridpoint distance) close to the excavations is 0.8 m. On the other hand, in the tunnel and shaft models, the mesh size in the shaft is 0.1 m. The Mohr-Coulomb (M-C) failure criterion with tension cut-off has been applied for the sandstone and the shale. In the classical M-C model the strength properties of the materials are assumed to remain constant after the onset of plastic failure. This assumption means that the material is able to support a stress equal to the failure strength after failure onset. The M-C failure criterion is given by Eq. (1).

$$f^s = \sigma_1 - \sigma_3 N_\phi + 2c\sqrt{N_\phi} \quad (1)$$

$$N_\phi = \frac{1 + \sin(\phi)}{1 - \sin(\phi)} \quad (2)$$

where f^s is the shear failure envelope, σ_1 and σ_3 are the major and minor principal stresses, ϕ is the friction angle and c is the cohesion. For the altered shale, the M-C ubiquitous-joint model has been applied. The M-C ubiquitous-joint is based on the M-C model, but in addition planes of weaknesses are taken into account. The M-C ubiquitous-joint failure criterion is given by Eq. (3).

$$f^s = \tau + \sigma_{33} \tan \phi_j - c_j \quad (3)$$

where ϕ_j , c_j , τ and σ_{33} are the friction, cohesion, tangential traction component and minor principal stress of the weakness plane, respectively. The plastic parameters are obtained by linearization of the generalized Hoek-Brown failure criterion (Hoek et al., 2002). Rock mass engineering properties for each lithology are obtained by means of the GSI rock mass classification under consideration of a disturbance factor (D).

Table 1
UPSH plant design parameters.

| UPSH design parameters | |
|--|---------|
| Lower reservoir – tunnels network (m^3) | 450,000 |
| Tunnels network (m) | 15,000 |
| Water flow rate ($\text{m}^3 \text{ s}^{-1}$) | 55 |
| Net head (kPa) | 3,864 |
| Turbine power (MW) | 190 |
| Air pressure - vent shaft 0.5 m ϕ (kPa) | 420 |
| Air pressure - vent shaft 1 m ϕ (kPa) | 120 |

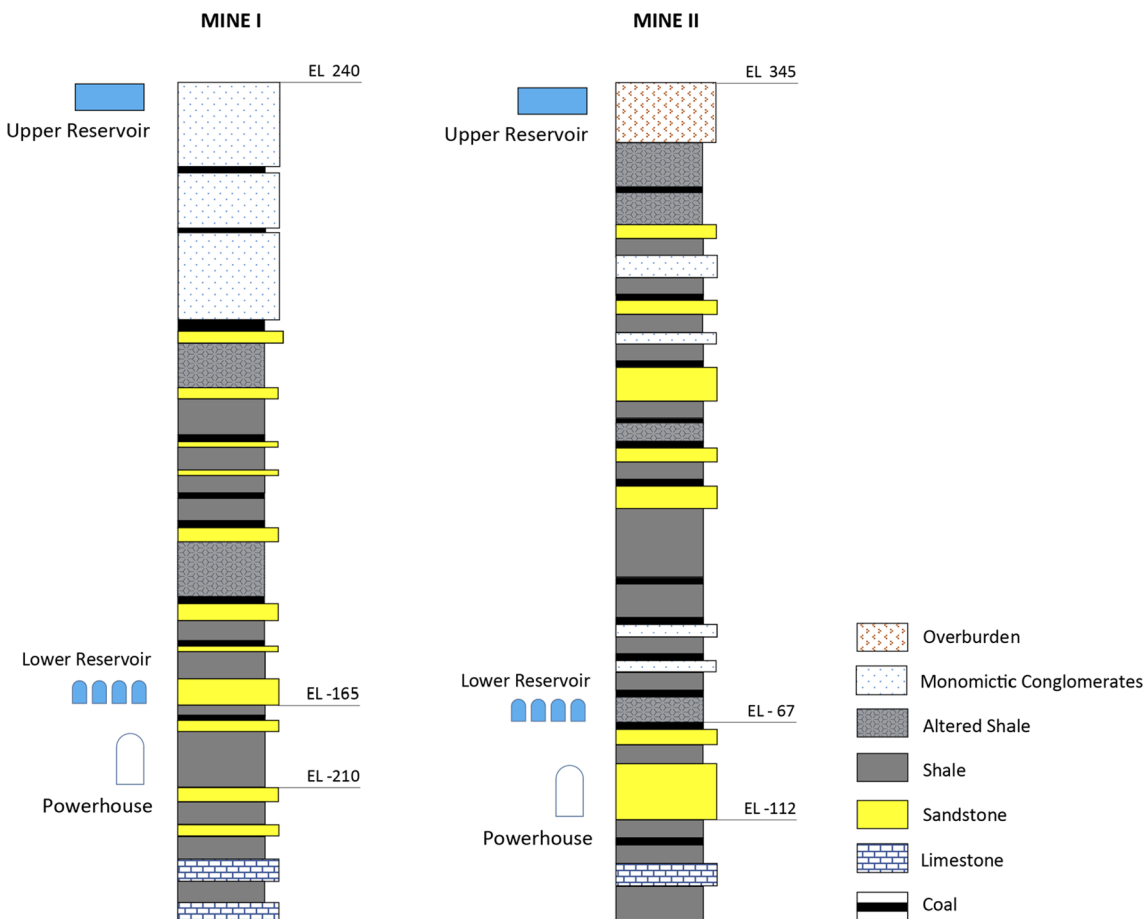


Fig. 3. Stratigraphic profiles for Mine I and Mine II. Powerhouse cavern and lower reservoir situation.

3.2. Material properties

Fig. 3 shows the stratigraphic profile of the Mine I and Mine II. In Mine I, the powerhouse cavern is excavated in sandstone at 450 m depth (EL -210 m a.s.l.). The lower reservoir is excavated in shale located at 405 m depth (EL -165 m a.s.l.). In Mine II, the powerhouse cavern is located at a depth of 457 m (EL -112 m a.s.l.), and it is excavated in shale. The excavation of the lower reservoir is performed in altered shale formation (affected by mining activities). The tunnel system of the lower reservoir is located at 412 m depth (EL -67 m a.s.l.).

HUNOSA coal mining company provided geological logs and rock mechanical data for the existing formations considered in the study area. The physical and mechanical properties of the rocks were determined by laboratory testing on intact rock samples following ISRM suggested methods (ISRM, 1981). Laboratory tests were performed on 40 core samples obtained from the case study mines at the University of Oviedo (Mechanics Laboratory). Brazilian tensile test, unconfined compressive strength (UCS) tests, triaxial compression test and direct shear test of discontinuities were conducted on the prepared samples to obtain the intact rock and discontinuity properties. Uncertainty has been considered by probability distributions for selected parameters. The relative standard uncertainty is lower than 9.7% and 8.3% for shale and sandstone samples, respectively. Uncertainty quantification has not been considered by the finite element model. Unfortunately, in-situ measurements are rare, however, several borehole pressiometer tests were conducted. They delivered the following values for the Young's modulus: 1.0–1.5 GPa for shale and 5.0–5.5 GPa for sandstone. These values are in close agreement with the parameters for Young's modulus derived from lab tests and rock mass classification.

The rock mass properties such as Hoek-Brown (H-B) constants, UCS

($\sigma_{c\text{mass}}$) and uniaxial tensile strength of rock mass ($\sigma_{t\text{mass}}$), deformation modulus (E_{mass}) and shear strength parameters were calculated by means of different empirical equations. The H-B failure criterion has been used to obtain the equivalent M-C strength parameters (cohesive strength and friction angle of rock masses). Unit weight (γ), intact uniaxial compressive strength (σ_{ci}), intact modulus (E_i), intact rock parameter (m_i), Geological Strength Index (GSI) and the constants used by the generalized H-B failure criterion (m_b , s and a) are given in Table 2. H-B constants (m_b , s and a) have been calculated by applying the following equations (Hoek et al., 2002):

$$m_b = \exp\left(\frac{GSI - 100}{28 - 14D}\right) \quad (4)$$

$$s = \exp\left(\frac{GSI - 100}{9 - 3D}\right) \quad (5)$$

$$a = \frac{1}{2} + \frac{1}{6} \left[\exp\left(\frac{-GSI}{15}\right) - \exp\left(\frac{-20}{3}\right) \right] \quad (6)$$

Table 2
Model parameters: intact rock properties, GSI and Hoek-Brown constants.

| Parameter | Shale | Sandstone | Altered shale |
|---|---------|-----------|---------------|
| Unit weight, γ (kN m ⁻³) | 23.83 | 25.87 | 23.83 |
| Intact Modulus, E_i (MPa) | 28,988 | 43,650 | 21,000 |
| Intact uniaxial comp. strength, σ_{ci} (MPa) | 59.7 | 150.8 | 35.0 |
| Intact rock constant (m_i) | 9.2 | 15.4 | 9.2 |
| GSI | 35 | 50 | 35 |
| m_b | 0.903 | 2.582 | 0.903 |
| s | 0.00073 | 0.00386 | 0.00073 |
| a | 0.5159 | 0.5057 | 0.5159 |

where m_b is a reduced value of the intact rock constant (m_i), s and a are rock mass constants. The intact rock constant (m_i) can be obtained by triaxial testing of rock. D is a factor that depends upon the degree of disturbance to which rock masses have been subjected by blast damage and stress relaxation. It varies from 0 for undisturbed in-situ rock masses to 1 for very disturbed rock masses. It has been assumed that the value of D is zero (excellent blasting quality).

Rock mass parameters, deformation modulus, E_{mass} (Hoek and Diederichs, 2006) and tensile strength of rock masses $\sigma_{t\text{mass}}$ (Hoek et al., 2002) have been calculated by applying Eq. (7) and Eq. (8), respectively.

$$E_{\text{mass}} = E_i \left(0.02 + \frac{1 - D/2}{1 + \exp^{((60+15D-GS)/11)}} \right) \quad (7)$$

$$\sigma_{t\text{mass}} = \frac{-s\sigma_{ci}}{m_b} \quad (8)$$

The equations for the friction angle φ' and cohesive strength c' of rock masses were given by Hoek et al. (2002):

$$\varphi' = \sin^{-1} \left[\frac{6\alpha m_b (s + m_b \sigma_{3n})^{\alpha-1}}{2(1+\alpha)(2+\alpha) + 6\alpha m_b (s + m_b \sigma_{3n})^{\alpha-1}} \right] \quad (9)$$

$$c' = \frac{\sigma_{ci} [(1+2\alpha)s + (1-\alpha)m_b \sigma_{3n}] (s + m_b \sigma_{3n})^{\alpha-1}}{(1+\alpha)(2+\alpha) \sqrt{1 + (6\alpha m_b (s + m_b \sigma_{3n})^{\alpha-1}) / ((1+\alpha)(2+\alpha))}} \quad (10)$$

where $\sigma_{3n} = \sigma_{\max} \sigma_{ci}^{-1} \sigma_{3\max}^{-1}$ is the upper limit of confining stress for which the relationship between the H-B and M-C criteria is considered. α is 0.16 for hard rocks and 0.35 for weak rocks. The corresponding rock mass properties are given in Table 3.

In altered shale formation, the planes of weakness are considered with a dip of 45° and a dip direction of 0°. To deduce the rock mass properties based on a rock mass classification a disturbance factor of $D = 0.8$ has been selected.

3.3. Numerical simulations

Six models were run for the two mines. For the powerhouse cavern models for Mine I and Mine II and the tunnel and shaft models for Mine

Table 3

Rock mass properties used for modelling Mine I and Mine II. The materials used in the simulations are indicated with bold text.

| Lithology | Young's modulus (MPa) | Poisson's ratio | Tensile strength (MPa) | Cohesion (MPa) | Friction angle (°) |
|---------------|-----------------------|-----------------|------------------------|----------------|--------------------|
| Overburden | 2,527 | 0.22 | 1.400 | 0.44 | 27.8 |
| Conglomerate | 8,200 | 0.23 | 3.300 | 5.54 | 22.4 |
| Limestone | 14,900 | 0.24 | 2.900 | 4.26 | 50.2 |
| Shale | 3,287 | 0.27 | 0.048 | 0.82 | 37.7 |
| Altered shale | 2,381 | 0.27 | 0.028 | 0.66 | 33.5 |
| Sandstone | 13,409 | 0.25 | 0.226 | 2.02 | 52.7 |
| Coal | 2,253 | 0.28 | 0.900 | 3.40 | 19.0 |

Table 4

Powerhouse cavern support system for shale and sandstone layers (Mine I and Mine II).

| Mine | Rock Mass | STAGE | Support system |
|---------|-----------|---------|---|
| MINE I | Shale | Crown | Systematic grouted rock bolts $\phi = 25$ mm, 225 kN, L = 6 m, Fibre reinforced shotcrete 200 mm, E = 10 GPa |
| | | Bench 1 | Systematic grouted rock bolts $\phi = 32$ mm, 350 kN, L = 15 m, Fibre reinforced shotcrete 200 mm, E = 10 GPa |
| | | Bench 2 | |
| | | Bench 3 | |
| MINE II | Sandstone | Crown | Systematic grouted rock bolts $\phi = 25$ mm, 225 kN, L = 6 m, Fibre reinforced shotcrete 100 mm, E = 10 GPa |
| | | Bench 1 | |
| | | Bench 2 | |
| | | Bench 3 | |

I and Mine II air pressure of 420 kPa and 120 kPa were considered for each mine. Shaft diameter was set to 0.5 m and 1 m in each mine.

For the powerhouse models, the following simulation steps were performed: (1) Generation of primary stress field by stepping towards model equilibrium and resetting deformations, (2) Excavation of caverns in 4 stages: top heading excavation and three bench excavations, and (3) Installation of support system immediately after excavation. State of plasticity and displacements values due to excavations and support measures were analyzed.

For tunnel and shaft models, the solution steps included: (1) Generation of primary stress field by applying vertical and horizontal stresses, (2) Excavation tunnels and shafts and (3) Application of air pressure of 420 and 120 kPa. Plastic zones and displacements values due to excavations and air pressure were analyzed.

The initial primary stress field at the powerhouse in a depth of 450 m is between 6.7 and 7.5 MPa in vertical direction and 2.2–2.5 MPa in horizontal direction. The in-situ horizontal stresses were estimated from empirical equations using global data and a compilation of local data for ACCB region.

3.4. Support system

From a first analysis and previous experience, the proposed support elements for each powerhouse cavern are summarized in Table 4. Systematic grouted rock bolts spaced 2 m and a layer of fibre reinforced shotcrete are considered in crown and walls. Particularly for underground powerhouse caverns, shotcrete's primary function is not only to limit the deformation of the rock mass but also to reduce groundwater seepage during construction and operation stages.

4. Results of numerical analysis

4.1. Powerhouse cavern stability

This section shows the results of the powerhouse simulations that have been carried out in unsupported and supported cases for Mine I and Mine II. The properties of support elements, such as rock bolt diameter, length, spacing, load capacity and thickness of shotcrete are given in Table 3.

4.1.1. Mine I

In Mine I, powerhouse cavern is excavated in shale. For unsupported and supported cases, the thickness of plastic zones and maximum total displacement at walls, roof and floor of the powerhouse cavern are shown in Fig. 4. The proposed support elements consist of systematic rock bolts: 25 mm diameter, 6 m long, spaced 2 m with wire mesh and 200 mm thick fibre reinforced shotcrete in crown (Stage 1); systematic rock bolts 32 mm diameter, 15 m long, spaced 2 m and 200 mm thick fibre reinforced shotcrete in walls (Stage 2, 3 and 4). Due to the thickness of the plastic zones, it was necessary to increase the length of the bolts up to 15 m in benches in excavation stages 2, 3 and 4. Fig. 4 shows the failure states for Mine I after reaching equilibrium. A combination of shear and tensile failure mechanisms are observed in the

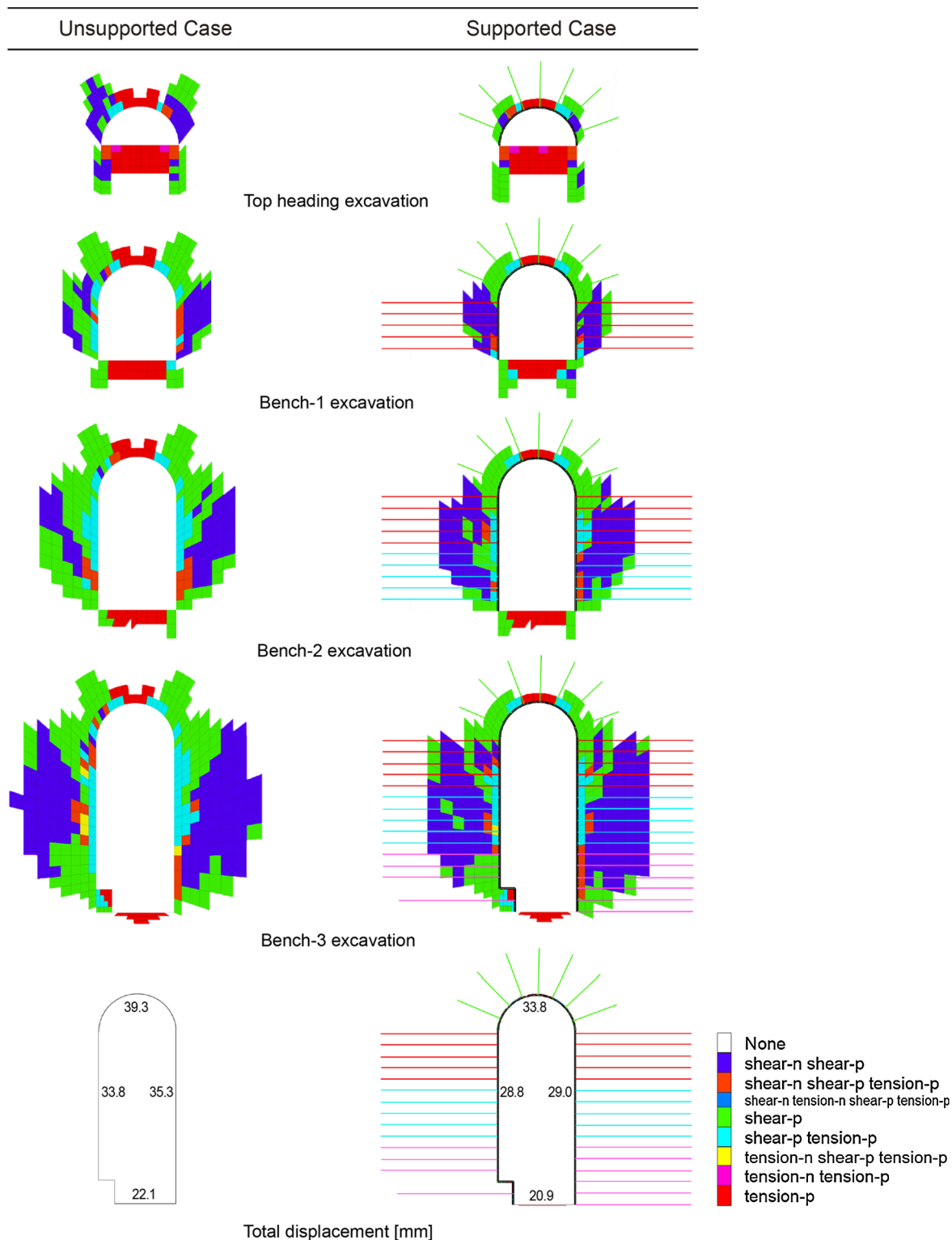


Fig. 4. Powerhouse cavern excavation stages in shale formation (Mine I). Failure states and total displacements in roof, walls and floor for unsupported and supported cases.

roof, the walls and the floor of the powerhouse cavern.

After support installation, the extension of the Excavation Disturbed Zone (EDZ) is reduced only slightly, however, the magnitude of displacements significantly decreased compared with the unsupported cases. The vertical displacement is reduced by 15% to 33.8 mm in the roof and the horizontal displacement is reduced by 18% to 28.8 mm in the walls.

The thickness of the plastic zone in the floor of the cavern is important, due to tensile failure in the first stage of excavation but decreases with ongoing excavation stages. Deformations for the unsupported case are similar to values obtained by the analytical elastic solution for a circular opening with 15 m diameter in an isotropic stress field.

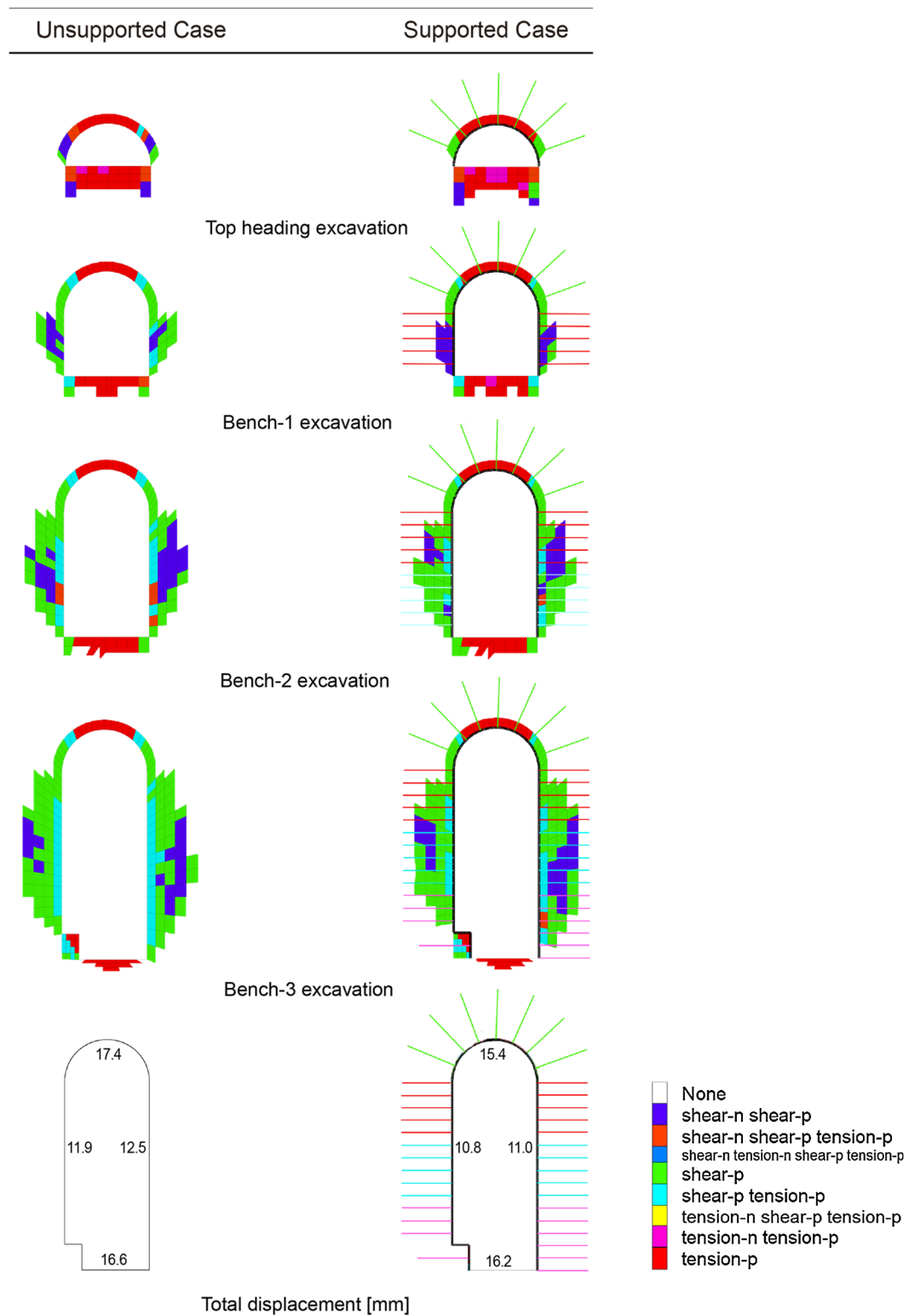


Fig. 5. Powerhouse cavern excavation stages in sandstone formation (Mine II). Failure states and total displacements in roof, walls and floor for unsupported and supported cases.

4.1.2. Mine II

The thickness of plastic zones and maximum total displacements in roof, walls and floor of the powerhouse cavern for unsupported and supported cases are shown in Fig. 5. In Mine II, the powerhouse cavern is excavated in sandstone. The proposed support system for the Mine II consist of systematic rock bolting: 25 mm diameter, 6 m long, spaced

2 m and 100 mm thick fibre reinforced shotcrete in crown and walls (Stage 1, 2, 3 and 4).

A combination of shear and tensile failure modes are observed in the roof of powerhouse caverns. In the walls, the failure modes change from a combination of shear and tensile failure to only shear failure. After support installation, the extension of the EDZ is reduced slightly, however, the

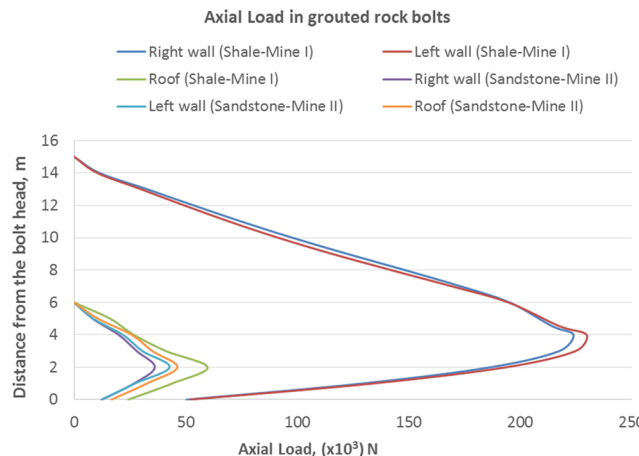


Fig. 6. Analysis of axial load in grouted rock bolts for Mine I and Mine II.

magnitude of displacements significantly decreased compared with the unsupported cases. The vertical displacement is reduced by 11% to 15.4 mm in the roof and the horizontal displacement is reduced by 12% to 10.8 mm in the walls. Again, deformations for the unsupported case are similar to values obtained by the analytical elastic solution for a circular opening with 15 m diameter in an isotropic stress field.

In summary, although the excavations are technically feasible with the designed support measures, in the Mine I (shale), due to bad quality of the rock mass, the thickness of the plastic zones around the cavern and the total displacements are quite big in all the excavation stages. In addition, the distribution of the axial force along the grouted rock bolts is considered as an important factor to adjust the rock bolt design (Imazu, 2000). Fig. 6 shows the axial load in grouted rock bolts for the caverns of Mine I and Mine II (shale and sandstone formations). Three bolt positions (roof, left wall and right wall) have been selected in each powerhouse cavern.

The maximum axial load is reached in the bolts of the cavern of Mine I (shale), with a value of 230 kN (left wall). The load capacity of the bolts designed for the cavern of Mine I is 350 kN. In the roof of the

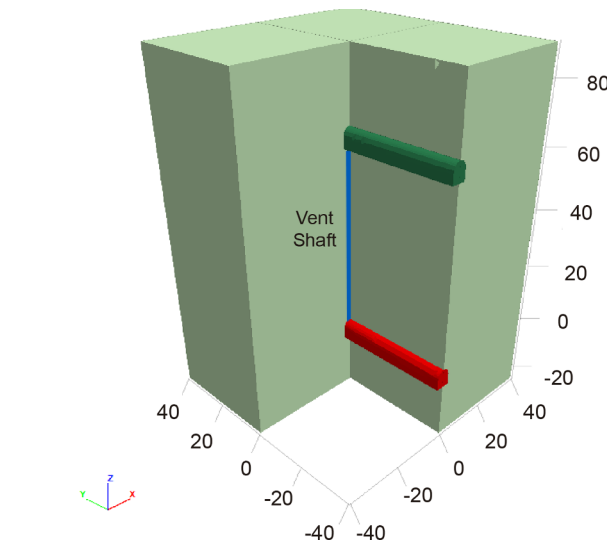


Fig. 8. Geometry of the tunnel and ventilation shaft model.

cavern in shale the axial load reaches only 59.9 kN. In the cavern of Mine II (sandstone) the axial load in the bolts are lower, with a maximum value of 46.3 kN in roof. In both caverns the designed load capacity is higher than the axial load reached in the rock bolts.

4.1.3. Numerical model validation

In-situ measurement data from Mine I and Mine II have been used to validate the proposed numerical model for powerhouse caverns in closed underground coal mines. Inclinometer data from two maintenance caverns - very similar in size compared to the planned powerhouse caverns - were used. Two inclinometers per cavern were installed from an above located drift at a distance of 2 and 4 m from the sidewalls of the cavern. After excavation, extensometers and convergence stations were also installed. The specific constellation was simulated and horizontal displacements in shale and sandstone formations have been compared with the in-situ measured data, with

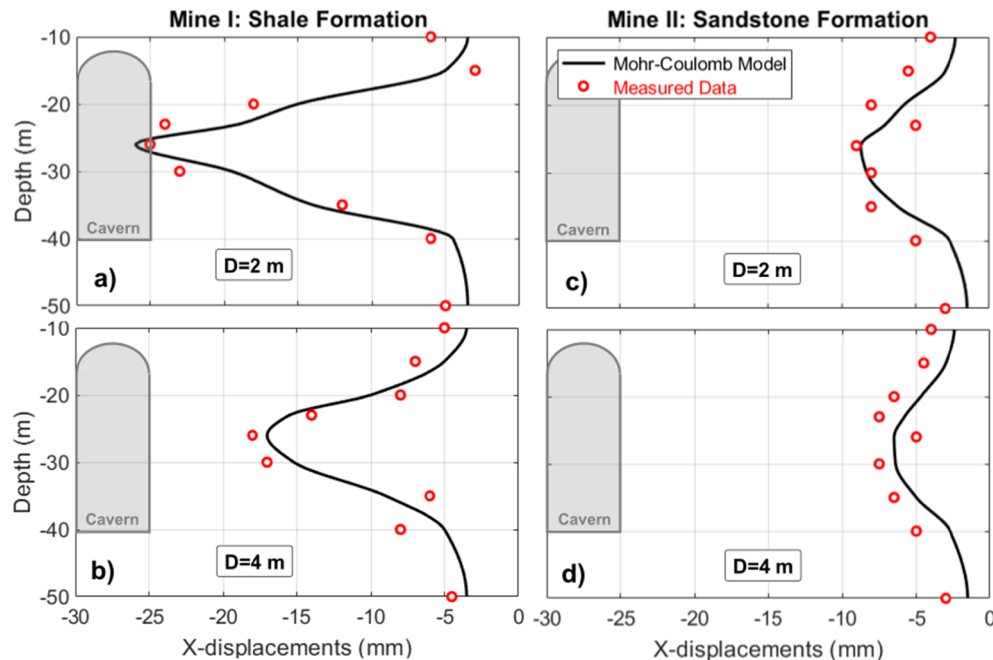


Fig. 7. Calculated vs. measured horizontal displacements at different distances. (a) 2 m from sidewall in shale; (b) 4 m from sidewall in shale; (c) 2 m from sidewall in sandstone; (d) 4 m from sidewall in sandstone.

reference to different distances from cavern sidewalls. Obtained results are shown in Fig. 7 for shale and sandstone formations (Mine I and Mine II).

Acceptable results have been obtained from this analysis. The numerical models duplicate the measured maximum horizontal displacements at a depth of half the cavern height ($h/2$). Also, the magnitudes and their distribution are well reproduced by the applied constitutive M-C model with the corresponding parameters.

4.2. Effect of air pressure on tunnels and shafts

In this section the results of the effect of the air pressure on the tunnels and shafts of the lower reservoir during the operation of the turbine are shown. Fig. 8 shows the geometry of the model. As indicated previously in Fig. 2, the model includes the lower reservoir tunnel, the ventilation shaft and the existing mine drift.

4.2.1. Mine I

The study has been carried out in two phases: construction phase and operation phase. In the Mine I, the tunnel and the intersection of the tunnel with the ventilation shaft is excavated in sandstone. Fig. 9 shows the failure states for Mine I after reaching equilibrium. The displacements caused by an air pressure of 420 kPa in tunnel and vent shaft with a diameter of 0.5 m are also given.

The thickness of the plastic zones is reduced in this model due to the quality of the rock mass. Shear failure mechanisms are observed in the tunnel. Tensile failure modes are insignificant. The excavation of vent shaft does not present shear or tensile failure. The results of the simulations show that the air pressure does not initiate a modification of the failure states. In Table 5 the results of the simulations in terms of

thickness of plastic zones and magnitude of displacements for both models in Mine I are shown. A displacement of 4.71 mm is reached during the excavation. In the operation stage, a displacement value of 0.16 mm is reached for air pressure of 420 kPa (0.5 m diameter). For an air pressure of 120 kPa, the displacement produced by the air pressure is reduced to 0.045 mm.

4.2.2. Mine II

In the Mine II, the tunnel and the intersection of the tunnel with the ventilation shaft is excavated in altered shale. In this model, a weak plane with a dip of 45° and a dip direction parallel to the tunnel axis has been considered. Fig. 10 shows the failure states and displacements caused by an air pressure of 420 kPa in tunnel and vent shaft with a diameter of 0.5 m.

A combination of shear and tensile failure in rock mass and weakness planes are observed. As for the model in sandstone, in this model the air pressure does not produce a change in the failure states. The thickness of the plastic zones reaches 2.6 m. In the model with a vent shaft of 1 m in diameter, an increase in the thickness of the plastic zones was observed at the junction of the ventilation shaft with the tunnel.

In Table 6 the results of the simulations in terms of thickness of plastic zones and displacements for both models in Mine II are given. A displacement of 73.9 mm is reached during excavation with a vent shaft of 0.5 m in diameter. If the diameter of the vent shaft is 1 m, the displacement during excavation reached 132.9 mm. To reduce these displacements, the installation of occasional rock bolts and a shotcrete layer is proposed. In the operation stage, the displacement caused by air pressure of 420 kPa is 0.91 mm. For an air pressure of 120 kPa, the displacement produced by the air pressure is only 0.26 mm.

During the operation phase the direction of the air flow switches

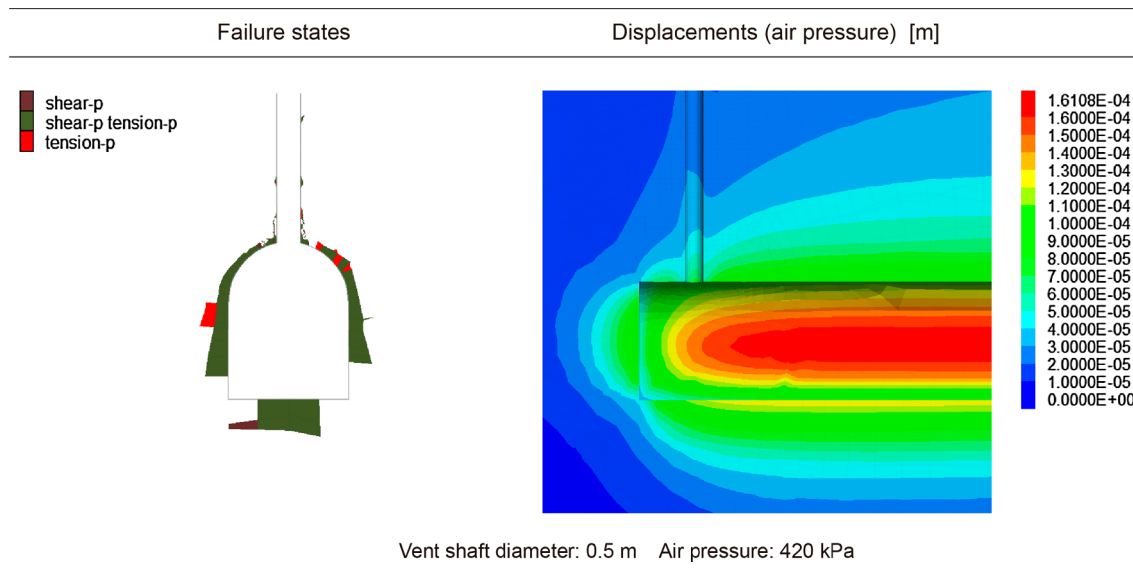


Fig. 9. Plastic zones (left) and displacements (right) caused by an air pressure of 420 kPa in tunnels and shaft in Mine I during operation time (sandstone formation).

Table 5

Thickness of plastic zones and maximum displacements caused by excavation and air pressure in tunnel and shaft for Mine I.

| STAGE | Vent shaft 0.5 m diameter (420 kPa) | | Vent shaft 1 m diameter (120 kPa) | |
|---------------------------|-------------------------------------|-------------------|-----------------------------------|-------------------|
| | Thickness of plastic zones [m] | Displacement [mm] | Thickness of plastic zones [m] | Displacement [mm] |
| Construction (Excavation) | 1.1 | 4.71 | 1.1 | 4.71 |
| Operation (Air pressure) | | 0.16 | | 0.045 |

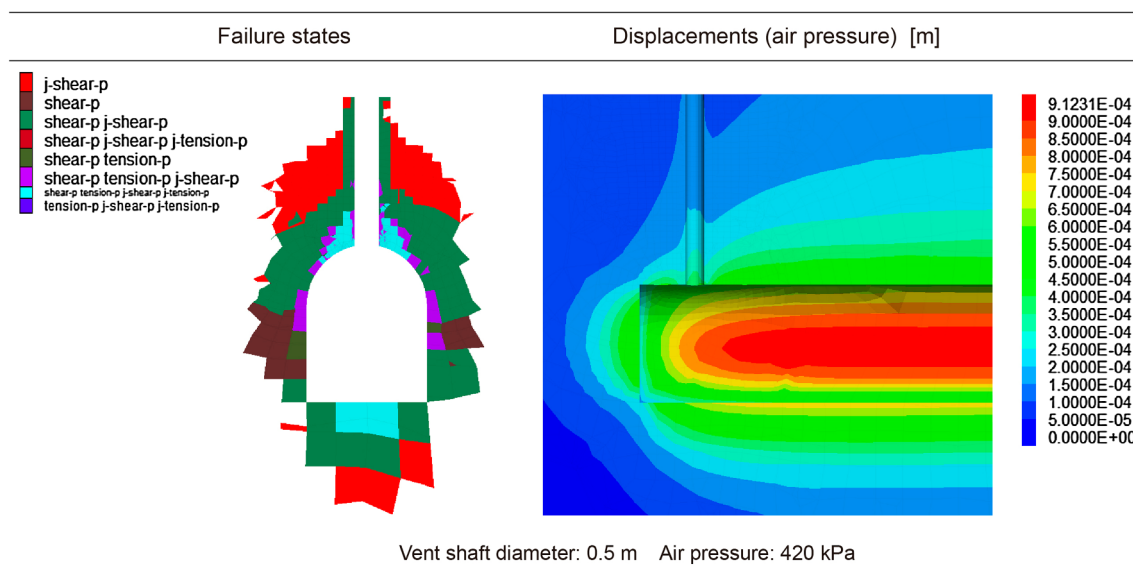


Fig. 10. Plastic zones (left) and displacements (right) caused by an air pressure of 420 kPa in tunnels and shaft in Mine II during operation time (altered shale formation).

Table 6

Thickness of plastic zones and displacement caused by excavation and air pressure in tunnel and shaft for Mine II.

| STAGE | Vent shaft 0.5 m diameter (420 kPa) | | Vent shaft 1 m diameter (120 kPa) | |
|---------------------------|-------------------------------------|-------------------|-----------------------------------|-------------------|
| | Thickness of plastic zones [m] | Displacement [mm] | Thickness of plastic zones [m] | Displacement [mm] |
| Construction (Excavation) | 2.6 | 73.88 | 2.6 | 132.95 |
| Operation (Air pressure) | | 0.91 | | 0.26 |

depending on the operating mode of the hydroelectric power plant: turbine or pumping mode. Due to these changes, the contour of the excavations is subjected to small cyclic tensile loads and damage at the microscopic scale could be produced. The long-term stability of the rock mass will depend on rock fatigue failure mechanisms (Guo et al., 2018; Song et al., 2018). To study the behavior of rock masses under cyclic loading, it would be necessary to carry out additional field measurements and laboratory tests on rock samples.

5. Conclusions

Closed underground coal mines are proposed as lower reservoir of UPSH plants. The excavation of the powerhouse cavern and a connected network of tunnels and shafts are necessary for the installation of the hydraulic equipment and the underground water lower reservoir, respectively. Due to the large cross section and the equipment installed inside, the stability of powerhouse caverns is one of the key requirements during construction and operation stages. In addition, during the operation phase an air flow is generated during the filling process of the lower reservoir. The air pressure can reach a value of up to 420 kPa. Therefore, it is necessary to analyze the effect of the air pressure on the stability of tunnels and ventilation shafts.

In summary, the research presented in this paper shows that the excavation of underground caverns in the ACCB for UPSH plants are technically feasible in the rock masses that have been analyzed. The thickness of the plastic zones as well as horizontal and vertical displacements are greater in the model of Mine I (shale). The support elements have been designed to reduce displacements in the four stages of excavation. The results of the numerical models show that no significant failure has to be expected in both mines. The predicted results are based on a validation of the constitutive law and its parameters using in-situ measurements in the mines.

The variations in air pressure during the operation of the facility have little effect on deformations and stability of the tunnels and ventilation shafts. In the model of the Mine II (altered shale) the displacements and the thickness of the plastic zones are higher due to the bad quality of the rock mass. In general, and supported also by this study, it is recommended to excavate vent shafts of 1 m diameter, where the air pressure is lower and the effects on the underground infrastructure are reduced. Due to changes in the direction of air flow, depending on the mode of operation (turbine or pumping), the rock mass is subjected to cyclic loading. If the ventilation shaft has a diameter of 0.5 m, a potential of long-term fatigue damage to the contours of the excavations exist, which needs further investigations.

Acknowledgements

Authors thank the mining company HUNOSA for providing geological and rock mechanical data.

References

- Braat, K.B., Van Lohuizen, H.P.S., De Haan, J.F., 1985. Underground pumped hydro-storage project for the Netherlands. *Tunnels Tunneling* 17 (11), 19–22.
- Fessenden, R.A., 1907. System of Storing Power, Application Filed June 7, 1,247,520 Patented Nov. 20, 191, 7, 1917.
- Guo, Y., Yang, C., Wang, L., Xu, F., 2018. Effects of cyclic loading on the mechanical properties of mature bedding shale. *Adv. Civil Eng.* 9, pp. <https://doi.org/10.1155/2018/8985973>.
- Hoek, E., Carranza-Torres, C., y Corkum, B., 2002. Hoek-Brown failure criterion – 2002 Edition, Proc. NARMS-TAC Conference, Toronto, 1, pp. 267–273.
- Hoek, E., Diederichs, M.S., 2006. Empirical estimation of rock mass modulus. *Int. J. Rock Mech. Min. Sci.* 43, 203–215.
- Ibrahim, H., Ilinca, A., Perron, J., 2008. Energy storage systems: characteristics and comparisons. *Renew. Sustain. Energy Rev.* 12 (5), 1221–1250. <https://doi.org/10.1016/j.rser.2007.01.023>.
- Imazu, M., 2000. Questions and answer about spray concrete and rock bolt. *Tunn. Undergr. Space Technol.* 31 (11), 87–88.

- ISRM, 1981. Rock characterization, testing and monitoring. ISRM Suggested Method, International Society for Rock Mechanics. Pergamon Press, Oxford.
- Kucukali, S., 2014. Finding the most suitable existing hydropower reservoirs for the development of pumped-storage schemes: an integrated approach. *Renew. Sustain. Energy Rev.* 37, 502–508.
- Luick, H., Niemann, A., Perau, E., Schreiber, U., 2012. Coalmines as underground pumped storage power plants (UPP) – a contribution to a sustainable energy supply? *Geophys. Res. Abstr.* 14, 4205.
- Menendez, J., Ordóñez, A., Álvarez, R., Loredo, J., 2019a. Energy from closed mines: underground energy storage and geothermal applications. *Renew. Sustain. Energy Rev.* 108, 498–512. <https://doi.org/10.1016/j.rser.2019.04.007>.
- Menendez, J., Loredo, J., Galdo, M., Fernandez-Oro, J.M., 2019b. Energy storage in underground coal mines in NW Spain: assessment of an underground lower water reservoir and preliminary energy balance. *Renew. Energy*, 134, 1381–1391. <https://doi.org/10.1016/j.renene.2018.09.042>.
- Menendez, J., Fernandez-Oro, J.M., Galdo, M., Loredo, J., 2019c. Pumped-storage hydropower plants with underground reservoir: influence of air pressure on the efficiency of the Francis turbine and energy production. *Renew. Energy*, 143, 1427–1438. <https://doi.org/10.1016/j.renene.2019.05.099>.
- Niemann, A., Perau, E., Schreiber, U., Erlich, I., Sures, B., Wagner, H.-J., Koch, M., Pielow, C., Weiss, M.-L., Fischer, P., 2015. Entwicklung eines Realisierungskonzeptes für die Nutzung von Anlagen des Steinkohlebergbaus als Unterirdische Pumpspeicherkraftwerke: Project Report FKZ 64.65.69-PRO-0039, Essen.
- Pendas, F., Loredo, J., 2006. El agua en los procesos de cierre de minas en Asturias. Proceedings of Reunión Científico-Técnica “Gestión del agua en los procesos de cierre de minas”. E.T.S. Ingenieros de Minas, University of Oviedo.
- Ray, A.K., 2009. Influence of cutting sequence on development of cutters and roof falls in underground coal mine. In: 28th International Conference on Ground Control in Mining, Morgantown, WV.
- Schoenung, S.M., Eyer, J.M., Iannucci, J.J., Horgan, S.A., 1996. Energy Storage for a competitive power market. *Annu. Rev. Energy Environ.* 21 (1), 347–370. <https://doi.org/10.1146/annurev.energy.21.1.347>.
- Severson, M.J., 2011. Preliminary evaluation of establishing an underground taconite mine, to be used later as a lower reservoir in a pumped hydro energy storage facility, on the Mesabi iron range, Minnesota: Natural Resources Research Institute, University of Minnesota, Duluth, MN, Report of Investigation NRRI/ RI-2011/02, 28p.
- Song, Z., Konietzky, H., Frühwirt, T., 2018. Hysteresis energy-based failure indicators for concrete and brittle rocks under the condition of fatigue loading. *Int. J. Fatigue* 114, 298–310. <https://doi.org/10.1016/j.ijfatigue.2018.06.001>.
- Tong, L., Liu, L., Yu, Q., Liu, S., 2013. Tunneling in abandoned coal mine areas: problems, impacts and protection measures. *Tunn. Undergr. Space Technol.* 38, 409–422. <https://doi.org/10.1016/j.tust.2013.07.020>.
- Uddin, N., Asce, M., 2003. Preliminary design of an underground reservoir for pumped storage. *Geotech. Geol. Eng.* 21, 331. <https://doi.org/10.1023/B:GEGE.0000006058.79137.e2>.
- Winde, F., Kaiser, F., Erasmus, E., 2016. Exploring the use of deep level gold mines in South Africa for underground pumped hydroelectric energy storage schemes. *Renew. Sustain. Energy Rev.* 78, 668–682. <https://doi.org/10.1016/j.rser.2017.04.116>.
- Wong, I.H., 1996. An underground pumped storage scheme in the bukit Timah granite of Singapore. *Tunn. Undergr. Space Technol.* 11 (4), 485–489.
- Yang, C.-J., Jackson, R.B., 2011. Opportunities and barriers to pumped-hydro energy storage in the United States. *Renew. Sustain. Energy Rev.* 15 (1), 839–844.